JOURNAL OF AIRCRAFT
Vol. 39, No. 2, March–April 2002

Numerical Investigation of Dynamic Stall Control via Airfoil Thickness Variation

Wandon Joo,* Kwanjung Yee,† and Dong-Ho Lee‡
Seoul National University, Seoul 151-742, Republic of Korea

Numerical experiments are conducted to investigate the effects of deformation control strategy in a dynamic stall control via active thickness variation. The aim is to clarify the dominant control parameters for an optimal thickness variation strategy. To achieve this goal, the thickness variation strategies are determined by superposing two components, a linear variation and a curved one. The effects of the control parameters on the lift stall angle, the moment stall angle, the maximum lift coefficient, and the maximum negative pitching moment are thoroughly examined. The results indicate that dynamic stall characteristics have a strong dependency on the thickness variation strategies of each phase. From the detailed analyses, it is found that 1) the variation strategies in the upstroke have a significant effect on the vortex formation at the leading edge and the vortex shedding speed is dependent of the thickness variation in the downstroke, 2) the dominant parameters in this control strategy are the sign and the magnitude of the curved variation, and 3) there exists an optimal thickness variation strategy to control of lift characteristics or moment characteristics.

Nomenclature

$C_{L\max}$	=	maximum lift coefficent
$C_{M\max}$	=	maximum pitching moment coefficent
T	=	maximum thickness of the airfoil at a given angle of attack
T_{curved}	=	sinuous thickness variation strategy, $T_{S\max} \times \sin[(\alpha-\alpha_1)/(\alpha_2-\alpha_1)\times\pi]$
$T_{L\max}$	=	thickness difference between $T_{1\max}$ and $T_{2\max}$
T_{linear}	=	linear thickness variation strategy, $T_{1\max}+(\alpha-\alpha_1)/(\alpha_2-\alpha_1)\times T_{L\max}$
$T_{S\max}$	=	amplitude of the sinuous thickness variation strategy function
T_{total}	=	final thickness variation strategy, $T_{\text{linear}}+T_{\text{curved}}$
$T_{1\max}$	=	maximum thickness of NACA0012 airfoil at 5-deg angle of attack
$T_{2\max}$	=	maximum thickness of NACA0016 airfoil at 25-deg angle of attack
$\alpha_{CL\max}$	=	angle of attack corresponding to the maximum lift coefficient
$\alpha_{CM\max}$	=	angle of moment coefficient was abruptly decreased
$\Delta T_{\max}$	=	ratio between the linear variation and the curved thickness variation, $T_{S\max}/T_{L\max}$
$\delta T/\delta\tau$	=	instantaneous velocity perturbation by the change of airfoil thickness

Subscripts

D	=	downstroke
U	=	upstroke

Introduction

DYNAMIC stall refers to a series of complicated aerodynamic phenomena accompanied by a stall delay of an airfoil in unsteady motion. In most cases, once the dynamic stall occurs, it may lead to an abrupt fluctuation of aerodynamic forces and impose excessive loads on structures. It is, therefore, regarded as a crucial factor that limits the ability of an aircraft or a helicopter to perform high-agility maneuvers. In past years, many experimental and numerical studies have been devoted to improve the aerodynamic characteristics of the dynamic stall, thereby to enlarge the flight envelope. All of such efforts can be roughly categorized as being either passive or active control measures to meet the goals.[1] Passive control methods are intrinsically unable to adjust to changing flowfields. Because of this, the active control methods have attracted more interest recently. Unlike passive control methods, active control strategies are based on the idea that the onset of flow separation might be delayed by directly supplying kinetic energy into the boundary layer, enhancing the turbulent entrainment rate. Conceptually, active control methods can be divided again into two categories, one for stationary and the other for moving control devices. Thus far blowing,[2,3] suction,[4–6] oscillatory surface heating,[7] and acoustic excitation[8] have been suggested for motionless devices. Examples in which motion of the control device is employed are moving surface,[9] buzz,[10] thickness variation,[11] oscillating flap,[12,13] and deformable leading edge.[14,15] The merits and demerits of each method can be found in the references.

Among the active control concepts mentioned, Geissler and Raffel have studied the feasibility of dynamic stall control via active thickness variation by means of numerical analysis and experiments.[11] The research results showed that the overall aerodynamic characteristics are greatly influenced by the strategies of the thickness variation. The concept of thickness variation is relatively simple and has an advantage of increasing the maximum lift without invoking the earlier drag divergence and moment stall.[11] Moreover, it becomes more possible to realize this concept judging from the current development of smart materials and flexible airfoil shell. As implied in Ref. 11, the remaining question is how to determine the appropriate control strategies of the thickness variation because the flowfields have quite different characteristics according to the control strategies even when the magnitudes of the allowable thickness variation are the same.

In this study, the general characteristics of aerodynamic responses according to the variations of control strategies are explored, and preliminary results are presented. The present research includes the following objectives: 1) investigation of aerodynamic characteristics according to the control strategies of thickness variations, 2) determination of the control parameters that have dominant influence on the characteristics of the flowfields, and 3) rough suggestion

Received 12 September 2000; revision received 6 June 2001; accepted for publication 7 June 2001.

*Graduate Student, School of Mechanical and Aerospace Engineering, Department of Aerospace Engineering; aerodon3@aerohel.snu.ac.kr.

†Research Fellow, Institute of Advanced Machinery and Design, Department of Aerospace Engineering; joelee@aerohel.snu.ac.kr.

‡Professor, School of Mechanical and Aerospace Engineering, Department of Aerospace Engineering; dhlee@gong.snu.ac.kr.

of the optimal strategy of thickness variation that can produce the best dynamic stall characteristics.

Numerical Methods

Governing Equations

Because dynamic stall includes complex aerodynamic phenomena such as massive separation and vortex shedding, two-dimensional unsteady Navier–Stokes equations are employed in this work:

$$\frac{1}{J}\frac{\partial \boldsymbol{Q}}{\partial t} + \frac{\partial \boldsymbol{E}}{\partial \xi} + \frac{\partial \boldsymbol{F}}{\partial \eta} = \frac{\partial \boldsymbol{E}_v}{\partial \xi} + \frac{\partial \boldsymbol{F}_v}{\partial \eta} \tag{1}$$

where, conservative variable vector $\boldsymbol{Q} = [\rho, \rho u, \rho v, \rho e, k, \omega]$.

The third-order upwind biased Roe's flux difference splitting (FDS) is used for spatial discretization. MUSCL with Koren limiter is also introduced to attain higher-order spatial accuracy. For temporal integration, Lower Upper-Symmetric Gauss Seidal (LU-SGS) is used together with dual time-stepping method.[16]

Until now, no turbulence model has been available to predict a massively separated flowfield with sufficient accuracy. The present study employs a baseline-SST (shear stress transport) turbulence model because it is known to yield relatively reliable results in the dynamic stall problem.[16] The baseline-SST turbulence model has been suggested by Menter as a mixed form of k–ε and k–ω model by way of the blending function F_1, which enables automatic switching to the appropriate model in response to the flowfield characteristics.[17] The details can be found in Ref. 17. It is known that the computational efficiency is better for the case that the turbulence calculation is sequentially performed after the flow solver. However, numerical convergency may become worse in such a sequential process. Therefore, in the present study, the turbulence routine is simultaneously solved with the flow solver.

The boundary conditions are specified as follows. On the solid wall the velocity is specified to the airfoil velocity to consider time-dependent motions. The pressure on the wall is evaluated from the normal momentum equation. At the inflow, freestream conditions are specified for velocity and pressure, and one-dimensional Riemann invariant extrapolation is used to obtain the density. At the outflow, freestream pressure is specified, and one-dimensional Riemann invariants are used to obtain the velocities and the density from the interior.

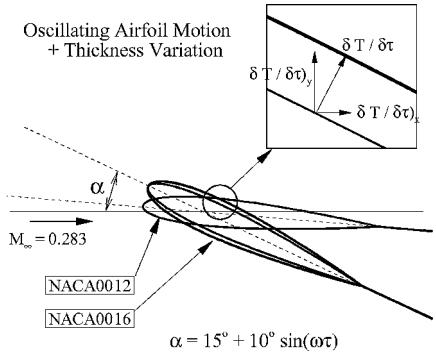

Fig. 1 Schematic of thickness variation on an oscillation airfoil.

Dynamic Grid System

When the body of interest undergoes geometric deformation with time, it would be necessary to reconstruct the grid system at each time step. However, because this would involve an excessive computational expense, the grid system has been obtained by a simple extrapolation technique suggested by Chyu et al. in Ref. 18. Therefore, at the end of the downstroke, the airfoil takes the shape of a NACA 0012 airfoil, whereas at the end of the upstroke it takes the shape of a NACA 0016 airfoil.

Figure 1 shows a simple schematic of the thickness variation procedure. It is clear from Fig. 1 that there exist velocity components orthogonal as well as parallel to the airfoil surface. Note that the time-dependent thickness variation generates not only a change in the geometric shape but also a velocity perturbation.

The thickness of the airfoil at a given time is determined by superposing the baseline linear thickness variation strategy (TVS) and the sinusoidal function as shown in Fig. 2:

$$T_{\text{total}} = T_{\text{linear}} + T_{\text{curved}} \tag{2}$$

$$\alpha = \alpha_1 + \alpha_2 \sin(\omega t) \tag{3}$$

$$T_{\text{linear}} = T_{1\,\max} + [T_{L\,\max}/(\alpha_2 - \alpha_1)](\alpha - \alpha_1)$$

$$T_{L\,\max} = T_{2\,\max} - T_{1\,\max} \tag{4}$$

$$T_{\text{curved}} = T_{S\,\max} \times \sin[(\alpha - \alpha_1)/(\alpha_2 - \alpha_1)\pi] \tag{5}$$

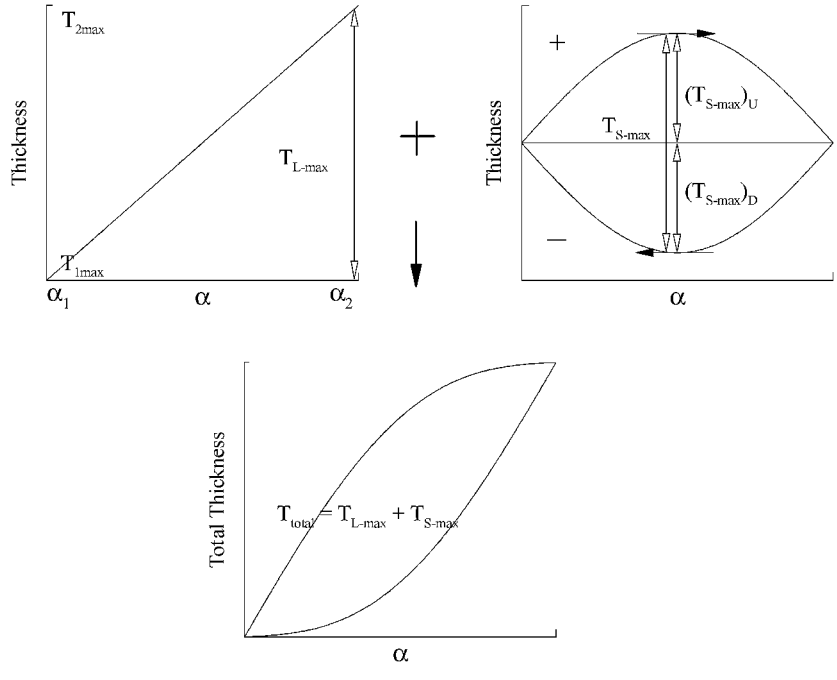

Fig. 2 Superposition of linear and curved TVSs.

Results and Discussions

Code Validation

The code has been validated for the oscillating NACA 0012 airfoil. The flow conditions are[19]

$$M_\infty = 0.283, \qquad \alpha = \alpha_0 + \alpha_m \sin(\omega\tau)$$

$$\alpha_0 = 15 \text{ deg}, \qquad \alpha_m = 10 \text{ deg}, \qquad Re = 3.45E6 \quad (6)$$

with reduced frequency

$$k = \omega/2M_\infty = 0.151 \quad (7)$$

Figure 3 shows the histories of the aerodynamic coefficients over a single period. The calculated maximum lift coefficient is 2.122 and shows good agreement with the experiment, 2.146. However, there is a slight discrepancy in the stall angle by 0.5 deg between the experiment (22.43 deg) and calculation (23.09 deg). Moreover, the calculated lift coefficients have slightly lower values during the upstroke phase than the experimental results. The calculation accuracy is found to be rather sensitive to the transition point in the turbulence model; it is already known that transition flow at the leading edge has a great effect on the ensuing development of overall unsteady flowfields.[20] At the early stage of the downstroke phase, the normal force increases due to the influence of trailing-edge vortex, and after it is separated from the airfoil, the normal force decreases gradually. The prediction accuracy in this region is very dependent on the choice of turbulence model. The baseline SST model is exclusively used in this study because, for the given flow conditions, some numerical oscillations are observed in the other two- equation models. The drag divergence angle and moment stall angles are also in good agreement with experiments.

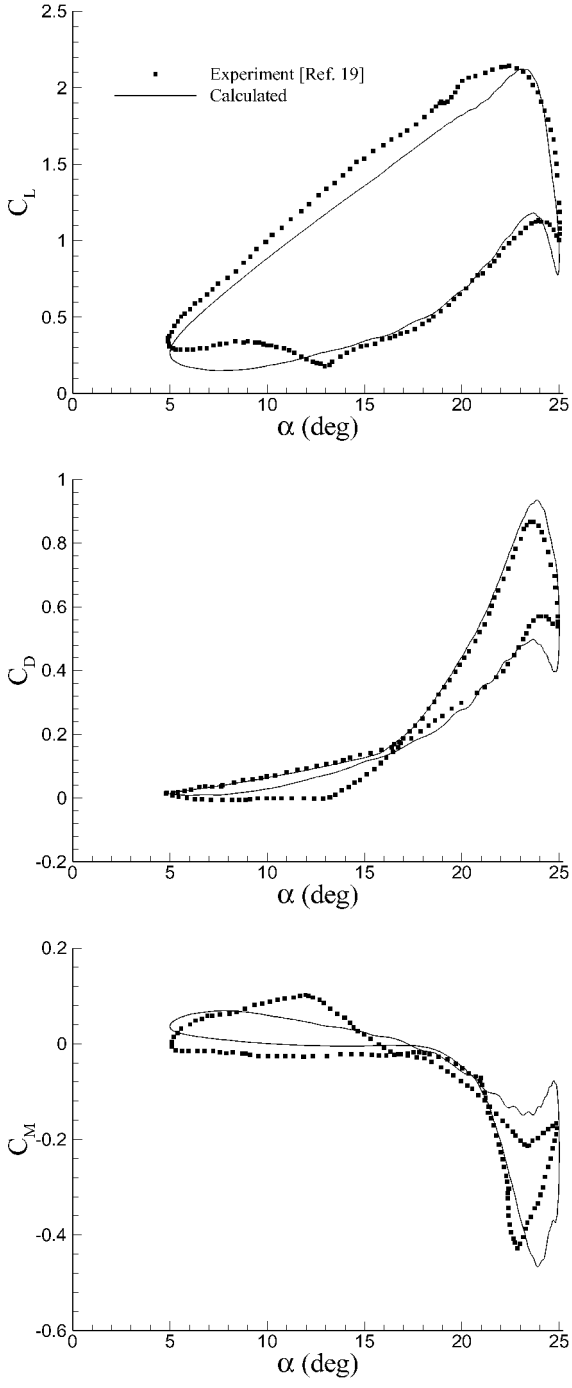

Fig. 3 Comparison of numerical solution with experiment: $M_\infty = 0.283$, $\alpha = 15$ deg + 10 deg sin($\omega\tau$), $Re = 3.45 \times 10^6$, and $k = \omega/2M_\infty = 0.151$.)

Classification of TVS

To classify the thickness variation, a new parameter is defined as follows:

$$\Delta T_{\max} = T_{S\max}/T_{L\max}, \qquad (\Delta T_{\max})_U = (T_{S\max})_U/T_{L\max}$$

$$(\Delta T_{\max})_D = (T_{S\max})_D/T_{L\max} \quad (8)$$

Additionally, two factors are taken into account for the given TVS: the maximum thickness of the airfoil at a given angle of attack and the instantaneous velocity perturbation added by the change of airfoil thickness, which are defined as

$$T = T(\tau^n) \quad (9)$$

$$\frac{\delta T}{\delta \tau} \cong \frac{T(\tau^n) - T(\tau^{n-1})}{\tau^n - \tau^{n-1}}, \qquad \tau^n = \tau^{n-1} + \Delta\tau \quad (10)$$

T is thought of as a geometric effect due to the active thickness control, whereas $\delta T/\delta\tau$ represents the corresponding velocity perturbation.

Influence of Upstroke TVS

Figure 4a shows a series of TVSs for the upstroke phase in which the downstroke TVS is kept constant along the baseline strategy, that is, $(\Delta T_{\max})_U \neq 0$ and $(\Delta T_{\max})_D = 0$. As arranged in Table 1, the TVSs are classified into three categories in terms of the magnitude and sign of $(\Delta T_{\max})_U$. For example, in case of positive $(\Delta T_{\max})_U$, the thickness variation rate is larger than that of the baseline at the beginning but smaller at the ending of the upstroke phase. The time rates of the thickness variation are shown in Fig. 4b for the corresponding $(\Delta T_{\max})_U$ to identify the velocity perturbation effects on the aerodynamic characteristics of dynamic stall. From the definition of $(\Delta T_{\max})_U$, this is totally due to the increase of $(T_{S\max})_U$ because $T_{L\max}$ and $(\Delta T_{\max})_D$ are kept constant in these cases.

The lift histories according to the various TVSs are shown in Fig. 5, from which it is clear that there is a substantial influence of the upstroke TVSs on the aerodynamic characteristics of the overall flowfields even when the linear thickness variation ranges $(\Delta T_{\max})_D$ are the same for each case.

For quantative analysis, the maximum lift coefficient $C_{L\max}$ and the corresponding angle of attack $\alpha_{CL_{\max}}$ are shown with respect to $(\Delta T_{\max})_U$ in Fig. 6. It shows that $C_{L\max}$ and $\alpha_{CL_{\max}}$ are proportional to the magnitude of $(\Delta T_{\max})_U$. The $\alpha_{CL_{\max}}$ reaches its maximum at

Table 1 Relative magnitude of each parameter in upstroke phase

Upstroke	Beginning	(5 ~ 15 deg)	Ending	(15 ~ 25 deg)
$(\Delta T_{\max})_U$	T	$\delta T/\delta\tau$	T	$\delta T/\delta\tau$
Positive	Large	Large	Large	Small
0	Base	Base	Base	Base
Negative	Small	Small	Small	Large

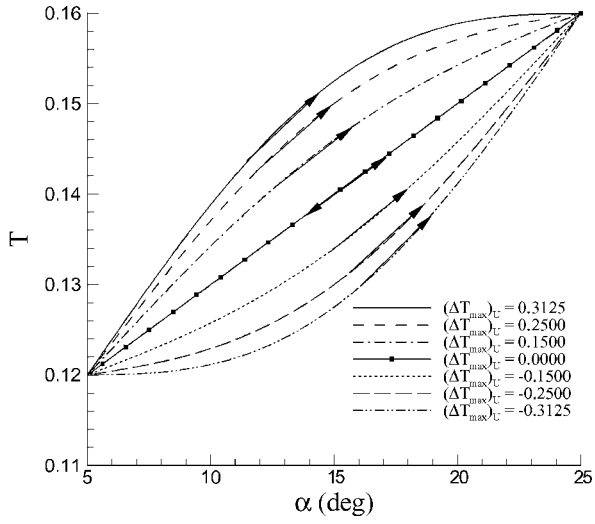

Fig. 4a Upstroke thickness variation with constant downstroke strategy [$(\Delta T_{max})_D = 0$].

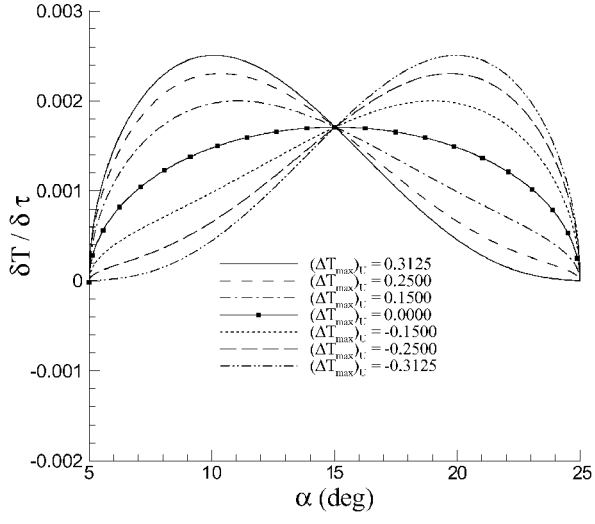

Fig. 4b Upstorke thickness variation rate with constant downstroke strategy [$(\Delta T_{max})_D = 0$].

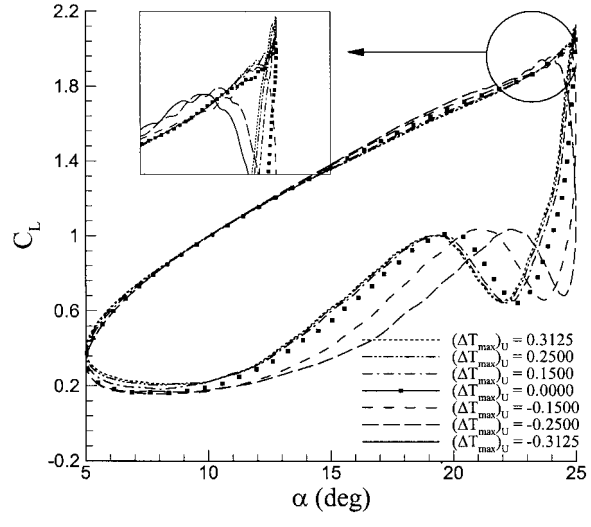

Fig. 5 C_L histories for the upstroke thickness variation.

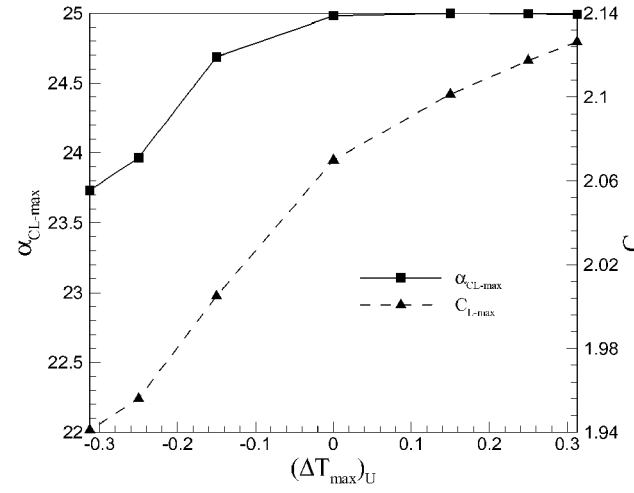

Fig. 6 Angle of attack $\alpha_{CL\,max}$ and $C_{L\,max}$ with respect to $(\Delta T_{max})_U$.

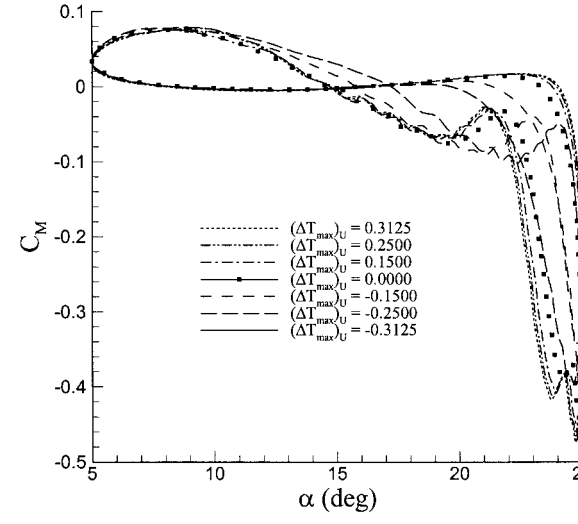

Fig. 7 C_M histories for the upstroke thickness variation.

the baseline case, that is, $(\Delta T_{\max})_U = 0$), and is kept constant irrespective of the increase of $(\Delta T_{\max})_U$, whereas the $C_{L\max}$ continues to increase, although the slope changes slightly. The stall angle is delayed by 1.3 deg, and $C_{L\max}$ increases by 0.2 compared with the worst case.

Figure 7 shows the moment histories with the variations of $(\Delta T_{\max})_U$. The relation between the moment stall angles and maximum negative moments are also shown in Fig. 8. It is found from Fig. 8 that the maximum negative moments decrease, whereas the moment stall angles are delayed with the increase of $(T_{S\max})_U$ That is, it is very hard to improve the characteristics of the moment stall angles and the maximum negative moments at the same time and this implies that a proper compromise is required to achieve the goal. Now, the question is, "*what makes the difference?*" The case of $(\Delta T_{\max})_U = 0.3125$ is found to have favorable characteristics in terms of the delay of lift and moment stall. However, it also increases the maximum negative moment and negative damping area, which has larger T and $\delta T/\delta\tau$ in the early stage of upstroke, whereas at the ending stage retains large T but small $\delta T/\delta\tau$ (Fig. 4b).

In the absence of adverse pressure gradient, the thicker airfoil may be useful to prevent leading-edge separation because it alleviates the abrupt suction peak around the airfoil nose. Moreover, for the relatively low angle of attack, below static stall angle of attack, the time-dependent thickness variation provides an additional velocity perturbation parallel as well as orthogonal to the freestream and enhances turbulent entrainment, as indicated in Fig. 1. However, once

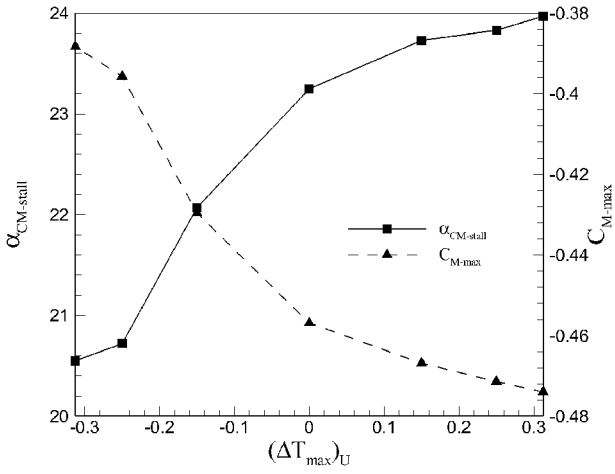

Fig. 8 Angle of attack $\alpha_{CM\,max}$ and $C_{M\,max}$ with respect to $(\Delta T_{max})_U$.

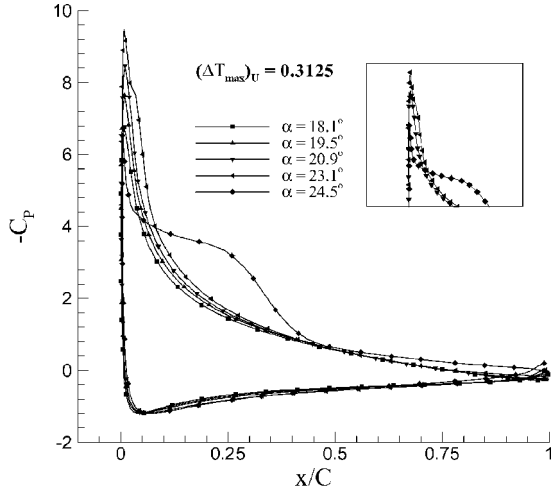

Fig. 9a C_P distributions where $(\Delta T_{max})_U = 0.3125$.

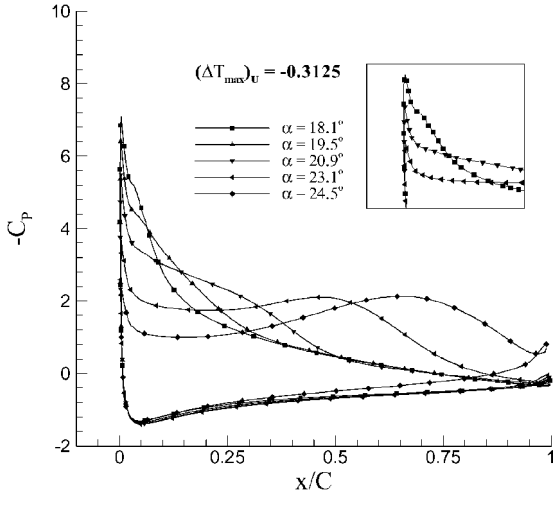

Fig. 9b C_P distributions where $(\Delta T_{max})_U = -0.3125$.

the vortex bubble forms at the leading-edge region, the velocity perturbation given by the thickness variation seems to have a tendency to accelerate vortex shedding. This accelerated vortex shedding creates a relatively strong vortex at the leading edge, resulting in the greater maximum negative moment. Also, because of delayed shedding, it takes longer for the shed vortex to pass through the moment center. Accordingly, the negative damping area increases. Therefore, in the case of $(\Delta T_{max})_U = -0.3125$, where $\delta T/\delta\tau$ has a higher

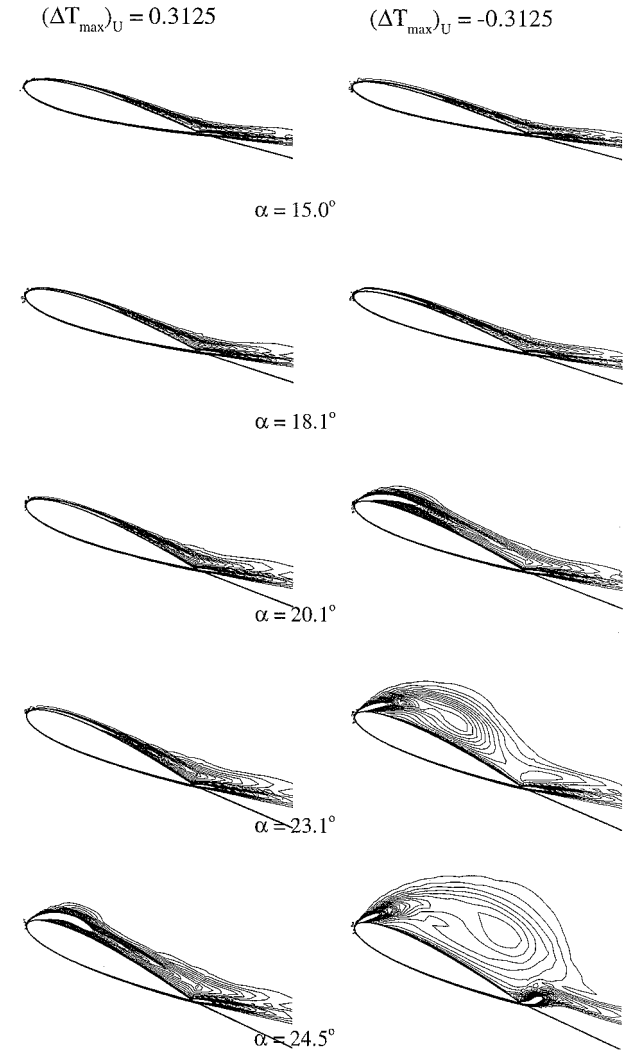

Fig. 10 Instantaneous vorticity contours: $M_\infty = 0.283$, $\alpha = 15$ deg + 10 deg $\sin(\omega\tau)$, $Re = 3.45 \times 10^6$, and $k = \omega/2M_\infty = 0.151$.

value at the ending stage of the upstroke, shedding occurs faster than the other cases. The instantaneous surface pressure distributions are shown Figs. 9a and 9b for the two extreme cases, $(\Delta T_{max})_U = 0.3125$ and $(\Delta T_{max})_U = -0.3125$. It is clearly shown that the stall onset and ensuing aerodynamic behaviors are quite different for the two cases. In case that $(\Delta T_{max})_U = 0.3125$, the onset of dynamic stall begins at around 23 deg, whereas the vortex bubble detaches at 18 deg for $(\Delta T_{max})_U = -0.3125$.

The successive vorticity contours of the two cases are shown in Fig. 10 to manifest the differences in the formation and shedding of the vortex bubble. From the discussion, it is found that a proper compromise is required because it is very hard to improve the characteristics of the lift and the pitching moment simultaneously.

Influence of Downstroke TVS

Similar computations are performed for TVSs in the downstroke phase. Figure 11a shows the various TVSs of the downstroke while the upstroke TVS is kept constant, that is, $(\Delta T_{max})_D \neq 0$ and $(\Delta T_{max})_U = 0$. The relative magnitudes of the two parameters are arranged with respect to the sign of $(\Delta T_{max})_D$ in Table 2. For example, in case that $(\Delta T_{max})_D$ is positive, the thickness variation rate is smaller than that of the baseline at the beginning but larger at the ending of the upstroke phase. The time rates of thickness variation for each case are shown in Fig. 11b.

Figure 12 shows the lift coefficient histories over a single cycle, where it is found that the TVS of the downstroke phase has little influence on the delay of dynamic stall but has some effects on the

Table 2 Relative magnitudes of each parameter in downstroke phase

Downstroke	Beginning	(25 ~ 15 deg)	Ending	(15 ~ 5 deg)
$(\Delta T_{\max})_D$	T	$\delta T/\delta\tau$	T	$\delta T/\delta\tau$
Positive	Large	Small	Large	Large
0	Base	Base	Base	Base
Negative	Small	Large	Small	Small

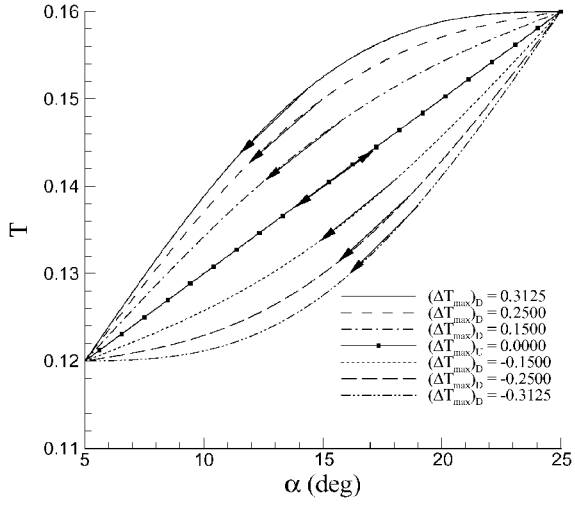

Fig. 11a Downstroke thickness variation with constant upstroke strategy [$(\Delta T_{\max})_U = 0$].

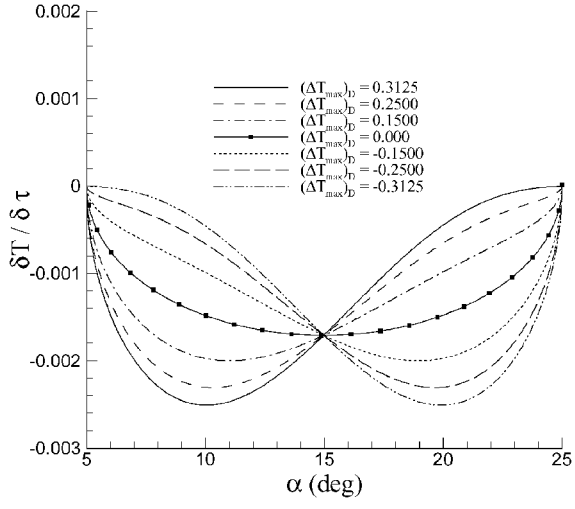

Fig. 11b Downstroke thickness variation rate with constant upstroke strategy [$(\Delta T_{\max})_U = 0$].

$C_{L\max}$ and the poststall characteristics. The $C_{L\max}$ and $\alpha_{CL\max}$ are shown with respect to $(\Delta T_{\max})_D$ in Fig. 13. As shown in Fig. 13, $\alpha_{CL\max}$ is practically independent of the mangitude of $(\Delta T_{\max})_D$. On the other hand, the magnitude of $C_{L\max}$ decreases almost linearly with $(\Delta T_{\max})_D$.

Figure 14 shows the moment histories with the variations of $(\Delta T_{\max})_D$. The relation between the moment stall angles and maximum negative moments are also shown in Fig. 15. The thickness variations at the downstroke phase have a stronger influence on the maximum negative moments and damping area rather than on the moment stall angles. This is because the vortex formation at the leading edge is not directly influenced by the downstroke thickness variations. Nevertheless, the maximum lift coefficient and the maximum negative moment have maximum values in the case of $(\Delta T_{\max})_D = -0.3125$, It is thought that the rapid decrease at the early phase of the downstroke has an effect to capture the vortex, as in the suction. Therefore, the case of $(\Delta T_{\max})_D = 0.3500$ is appropriate simply to improve the moment characteristics.

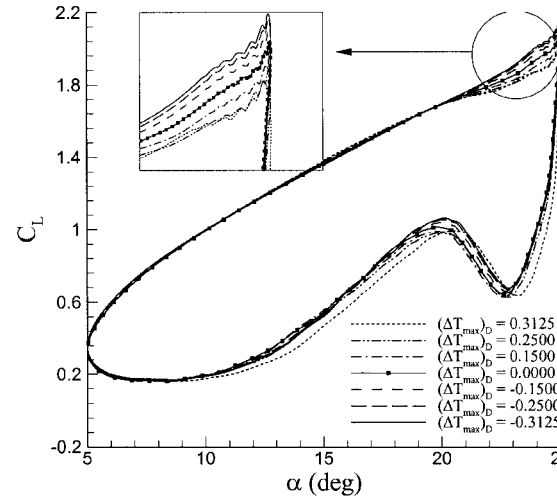

Fig. 12 C_L histories for the downstroke thickness variation.

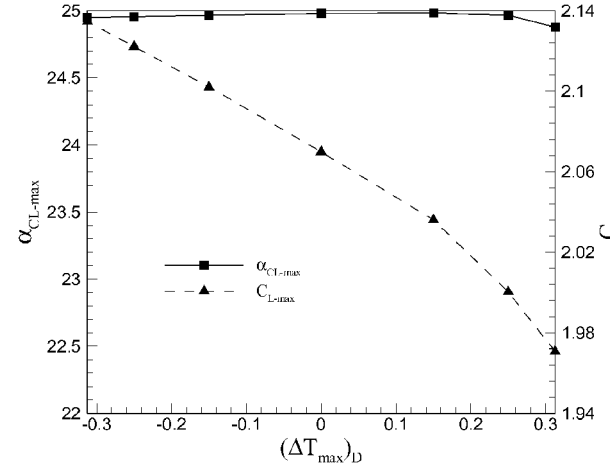

Fig. 13 Angle of attack $\alpha_{CL\max}$ and $C_{L\max}$ with respect to $(\Delta T_{\max})_D$.

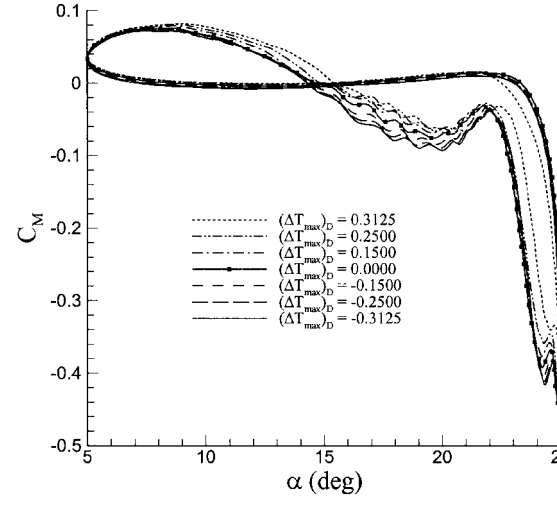

Fig. 14 C_M histories for the downstroke thickness variation.

Figures 16a and 16b show the surface pressure distributions of $(\Delta T_{\max})_D = 0.3125$ and $(\Delta T_{\max})_D = -0.3125$. In the case of $(\Delta T_{\max})_D = 0.3125$, the stall onsets at about 19.5 deg, whereas a vortex bubble initiates on the airfoil surface at 21 deg for $(\Delta T_{\max})_D = -0.3125$.

Suggestion of Proper TVS

With these lessons in mind, a better TVS has been suggested. To obtain a higher stall angle and $C_{L\max}$, the time rate of thickness

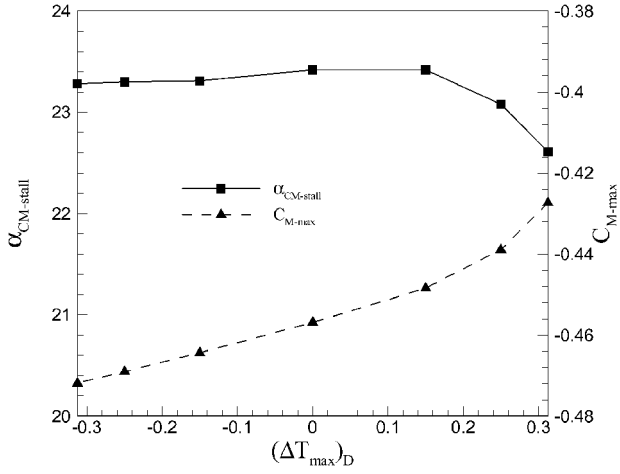

Fig. 15 Angle of attack $\alpha_{CM\,max}$ and $C_{M\,max}$ with respect to $(\Delta T_{max})_D$.

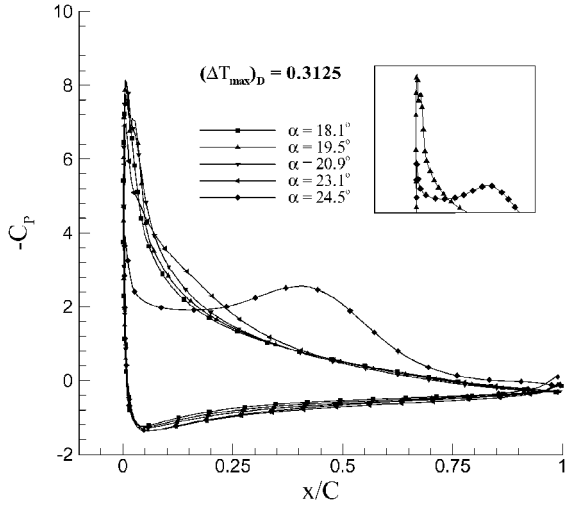

Fig. 16a C_P distribution where $(\Delta T_{max})_D = 0.3125$.

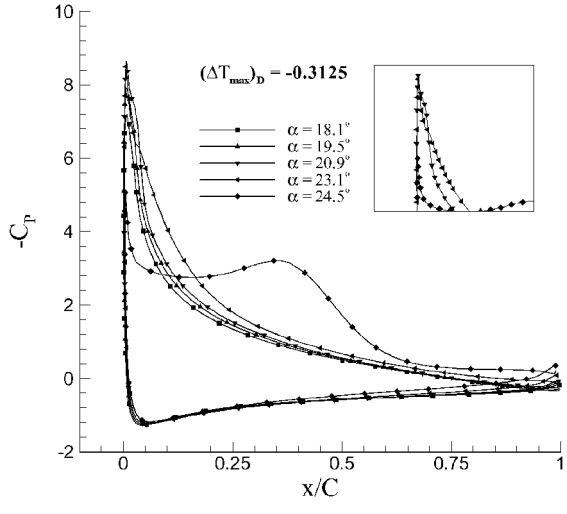

Fig. 16b C_P distribution where $(\Delta T_{max})_D = -0.3125$.

variation should be kept high at the early stages of each phase, whereas the opposite is true at the end of each phase, as shown in the inset of Fig. 17. In other words, a better lift performance is obtained with the increase of $(\Delta T_{max})_U$ during the upstroke. However, a smaller $(\Delta T_{max})_D$ is preferable for better lift performance during the downstroke. The comparisons of the lift coefficient histories are made between the baseline case and the present one.

Lift stall incidence is delayed by about 2 deg (8.5%) and the maximum lift coefficient increases by 0.06 (3%) in the lift-based

Table 3 Aerodynamic coefficients between suggested strategy and NACA 0012

Case	Lift stall angle	$C_{L\,max}$	Moment stall angle	$C_{M\,max}$
NACA 0012	23.05	2.1216	19.42	−0.4663
$\Delta T_{max} = 0.6250$ (lift based)	24.99	2.1854	23.80	−0.4898
$\Delta T_{max} = -0.3000$ (moment based)	24.43	1.9596	21.70	−0.4071

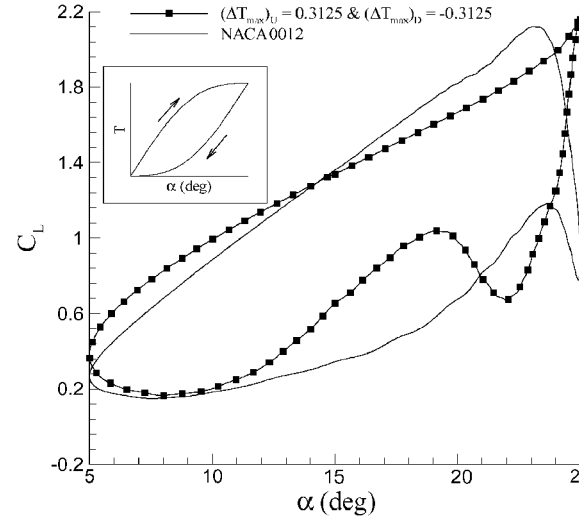

Fig. 17 C_L histories between the lift-based strategy and NACA 0012 cases.

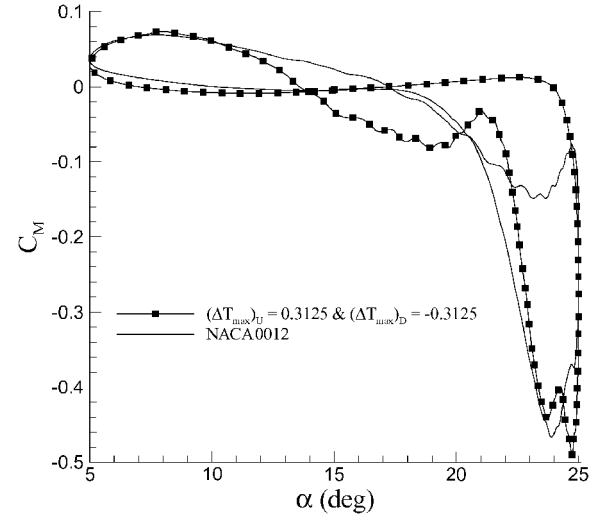

Fig. 18 C_M histories between the lift-based strategy and NACA 0012 cases.

TVS (see to Table 3). Moreover, note that hysteresis is significantly reduced due to the earlier reattachment.

The snapshots of vorticity contours are shown in Fig. 17 for the two cases mentioned earlier. As shown in Fig. 19, a vortex bubble begins to form at around 18.1 deg and sheds at 20.9 deg for the NACA 0012, whereas, in the $\Delta T_{max} = 0.6250$ case, the flow remains attached even at 24.5 deg. The resulting pitching moment histories are shown in Fig. 18. The moment stall angle is delayed by 4.4 deg, but the maximum negative pitching moment coefficient and the negative damping area increase. In general, the smaller negative damping area is preferable because it may avoid structural problems.

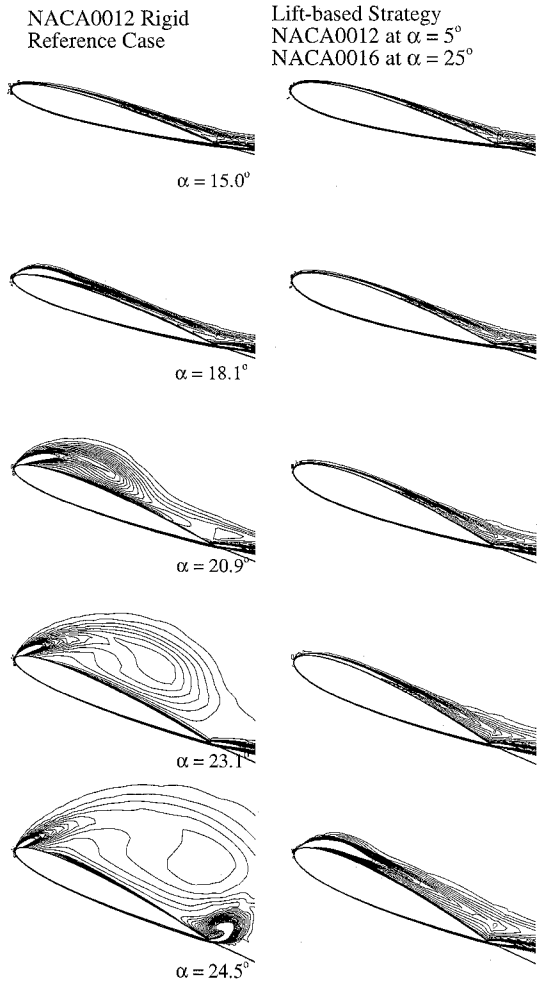

Fig. 19 Comparison of vorticity contours between lift-based strategy and NACA 0012 case.

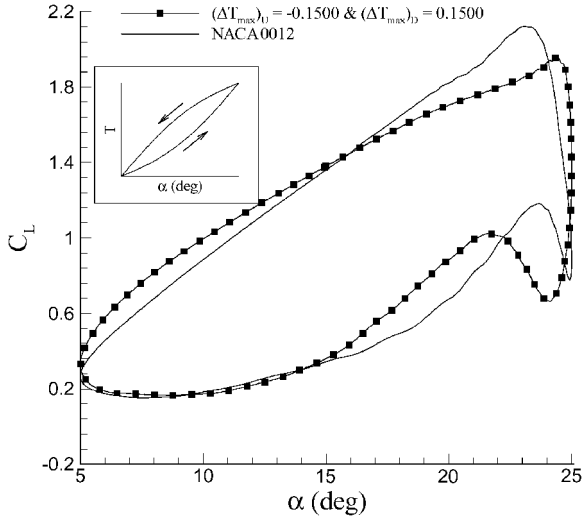

Fig. 20 C_L histories between the moment-based strategy and NACA 0012 cases.

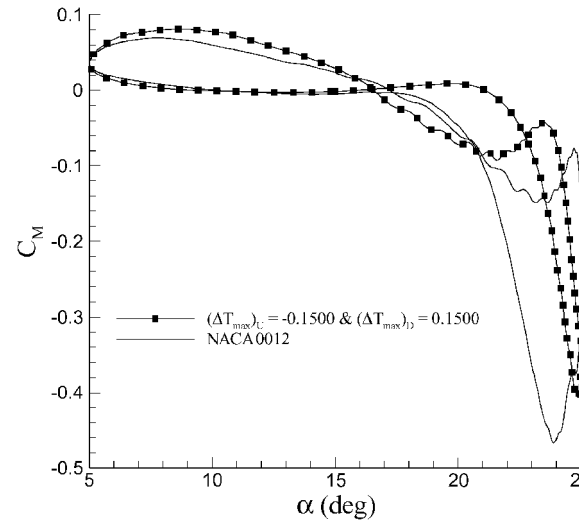

Fig. 21 C_M histories between the moment-based strategy and NACA 0012 cases.

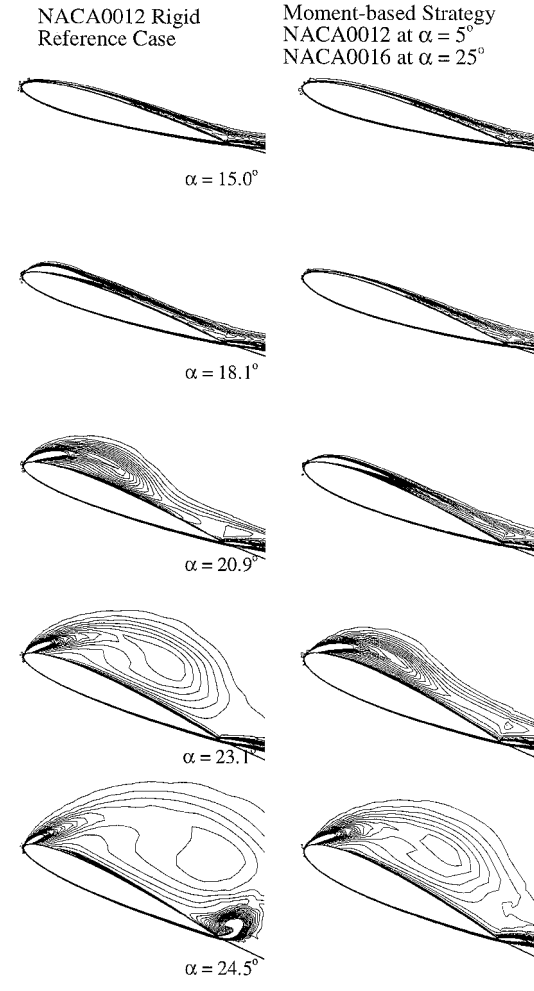

Fig. 22 Comparison of vorticity contours between moment-based strategy and NACA 0012 case.

In that sense, TVS is not always advantageous to increase the maximum lift coefficient.

To improve the pitching moment characteristics, one must consider the moment stall angle and the maximum negative pitching moment together with a negative damping area. At the upstroke phase, the case of $(\Delta T_{\max})_U = -0.1500$ has been chosen, where both the moment stall angle and the maximum negative moment have a moderate value. At the downstroke phase, the case of $(\Delta T_{\max})_D = 0.1500$ has been applied to minimize the maximum negative pitching moment with early moment stall. The lift and moment histories are summarized in Figs. 20 and 21 and Table 3. As can be seen from Figs. 20 and 21, the pitching moment characteristics have been improved by reducing the maximum negative pitching moment and the negative damping area, although the maximum lift coefficient has been decreased.

A comparison of the vorticity contours in the moment-based strategy and in the NACA 0012 case is shown in Fig. 22.

Conclusions

In this study, through a series of numerical calculations, it is found that the TVSs have a substantial effect on the aerodynamic characteristics of the overall flowfields and they can be used as an efficient control method if the control strategies are prudently selected.

1) The upstroke TVS has a significant effect on the vortex formation at the leading edge, whereas the downstroke TVS has one on the shedding velocity of the vortex.

2) For the higher maximum lift coefficient, the lift stall delay, and the moment stall delay, thickness variation rate should take a large value in the early stage of up- and downstroke. However, for small maximum negative pitching moment and the negative damping area, it should take a small value in early stage of each phase.

3) There exists a tradeoff relation between the stall delay and the pitching moments. This implies that a proper compromise should be made when applying TVS.

Acknowledgments

The authors gratefully acknowledge that this work was supported by the Brain Korea 21 Project in 2001. Special thanks are given for the support of the Center of Innovative Design Optimization Technology (Engineering Research Center (ERC) of Korea Science and Engineering Foundation).

References

[1]Gad-el-Hak, M., "Control of Low-Speed Airfoil Aerodynamics," *AIAA Journal*, Vol. 28, No. 9, 1990, pp.1537–1552.

[2]Katz, Y., Horev, E., and Wygnanski, I., "The Forced Turbulent Wall Jet," *Journal of Fluid Mechanics*, Vol. 242, 1992, pp. 577–609.

[3]Seifert, A., Bachar, T., Wygnanski, I., Koss, D., and Shepshelovich, M., "Oscillatory Blowing, a Tool to Delay Boundary Layer Separation," *AIAA Journal*, Vol. 31, No. 11, 1993, pp. 2052–2060.

[4]Wagner, R. D., and Fischer, M. C., "Fresh Attack on Laminar Flow," *Aerospace America*, Vol. 22, 1984, pp. 72–76.

[5]Wagner, R. D., Maddalon, D. V., and Fischer, M. C., "Technology Development for Laminar Boundary Control on Subsonic Transport Aircraft," CP-365, AGARD Paper 16, 1984.

[6]Karim, M. A., and Acharya, M., "Suppression of Dynamic-Stall Vortices over Pitching Airfoils by Leading-Edge Suction," *AIAA Journal*, Vol. 32, No. 8, 1994, pp. 1647–1655.

[7]Bayliss, A., Maestrello, L., Parikh, P., and Ting, L., "Numerical Simulation of Boundary Layer Excitation by Surface Heating/Cooling," *AIAA Journal*, Vol. 24, No. 7, 1986, pp. 1095–1101.

[8]Ahuja, K. K., Whipkey, R. R., and Jones, G. S., "Control of Turbulent Boundary Layer Flows by Sound," AIAA Paper 83-0726, 1983.

[9]Modi, V. J., "Moving Surface Boundary-Layer Control: A Review," *Journal of Fluids and Structures*, Vol. 11, 1997, pp. 627–663.

[10]Choi, S., "The Active Control of Boundary Layer Separation via Periodic Buzzing on the Airfoil Surface," M.S. Thesis, Dept. of Mechanics and Aero Engineering, Seoul National Univ., Seoul, Republic of Korea, Feb. 1998.

[11]Geissler, W., and Raffel, M., "Dynamic Stall Control by Airfoil Deformation," *19th European Rotorcraft Forum*, Cernobio, Italy, Paper C2, 14–16 Sept. 1993.

[12]Shepshelovich, M., Koss, D., Wygnanski, I., and Seifert, A., "An Experimental Evaluation of Low Reynolds number High-Lift Airfoil with Vanishingly Small Pitching Moment," *AIAA 27th Aerospace Sciences Meeting*, AIAA Paper 89-0538, Jan. 1989.

[13]Geissler, W., Sobieczky, H., and Vollmers, H., "Numerical Study of the Unsteady Flow on a Pitching Airfoil with Oscillating Flap," *24th European Rotorcraft Forum*, Marseilles, France, Paper AE09, 15–17 Sept. 1998.

[14]Chandrasekhara, M. S., Wilder, M. C., and Carr, L. W., "Unsteady Stall Control Using Dynamically Deforming Airfoils," *AIAA Journal*, Vol. 36, No. 10, 1998, pp. 1792–1800.

[15]Lee, S., McAlister, K. W., and Tung, C., "Characteristics of a Deformable Leading Edge for High Performance Helicopter Rotor," *AIAA 11th Applied Aerodynamics Conference*, AIAA Paper 93-3526, Monterey, CA, Aug. 1993.

[16]Lee, B., Lee, S., and Lee, D., "A Modification of SST Turbulent Model for the Analysis of Oscillating Airfoil," Annual Conf. of Korean Computational Fluid Dynamics Society, Vol. 4, No. 3, 1999, pp. 131–136.

[17]Menter, F. R., "Two-Equation Eddy-Viscosity Turbulence Models For Engineering Applications," *AIAA Journal*, Vol. 32, No. 8, 1994, pp. 1598–1605.

[18]Chyu, W. J., Davis, S. S., and Chang, K. S., "Calculation of Unsteady Flow over an Airfoil," *AIAA Journal*, Vol. 19, No. 6, 1981, pp. 684–690.

[19]McCroskey, W. J., McAlister, K. W., Carr, L. W., and Pucci, S. L., "An Experimental Study of Dynamic Stall on Advanced Airfoil Section," Vol. 1–3, NASA TM 84245, 1982.

[20]Wu, J.-C., Huff, D. L., and Sankar, L. N., "Evaluation of Three Turbulence Models in Static Air Loads and Dynamic Stall Predictions," *Journal of Aircraft*, Vol. 27, No. 4, 1990, pp. 382–384.